Systems & Control Transactions

Research Article - Peer Reviewed Conference Proceeding
ESCAPE 35 - European Symposium on Computer Aided Process Engineering
Ghent, Belgium. 6-9 July 2025
Jan F.M. Van Impe, Grégoire Léonard, Satyajeet S. Bhonsale,
Monika E. Polańska, Filip Logist (Eds.)

PSE PRESS

Thermo-Hydraulic Performance of Pillow-Plate Heat Exchangers with Streamlined Secondary Structures: A Numerical Analysis

Reza Afsahnoudeh[a], Julia Riese[a], Eugeny Y. Kenig[a]*

[a] Paderborn University, Chair of Fluid Process Engineering, Paderborn, Germany
* eugeny.kenig@upb.de.

ABSTRACT

Pillow-plate heat exchangers (PPHEs) represent a viable alternative to conventional shell-and-tube and plate heat exchangers. The waviness of their channels intensifies fluid mixing in the boundary layers and facilitates heat transfer. Applying secondary surface structuring can further enhance the overall thermo-hydraulic performance of PPHEs, thus increasing their competitiveness against conventional heat exchangers. In this work, streamlined secondary structures applied on the PPHE surface were studied numerically to explore their potential in enhancing near-wall fluid mixing. Computational fluid dynamics (CFD) simulations of single-phase turbulent flow in the inner PPHE channel were performed and pressure drop, heat transfer coefficients, and overall thermo-hydraulic efficiency were determined. The simulation results clearly demonstrate a favourable influence of secondary structuring on the heat transfer performance of PPHEs.

Keywords: Computational Fluid Dynamics, Surface structuring, Heat transfer intensification

INTRODUCTION

Pillow-plate heat exchangers (PPHEs) are a promising alternative to conventional shell-and-tube and plate heat exchangers. PPHEs are formed by assembling multiple pillow plates (PPs) into a single unit. These PPs are manufactured by spot-welding two steel sheets and seam-welding along the edges, followed by hydroforming, resulting in characteristic pillow-like surfaces (see Fig. 1).

Piper et al. [2] conducted a CFD-based study of turbulent fluid flow in the inner channels (IC) of PPs. Their simulation results revealed that a fully developed turbulent flow in PPs is characterized by two zones: a recirculation zone arising in the wake of a welding spot and a core flow confined by the wall and the recirculation zones. The recirculation zones increase pressure drop and are characterized by slow heat transfer. By reducing the size of these zones, the performance of the PPHEs can be improved; thus, optimization of the PPHE geometry is possible. Therefore, Piper et al. [2] investigated the effect of the form and size of welding spots on the thermo-hydraulic performance of PPHE inner channels. They reported a 37% efficiency increase for a PPHE with streamlined oval-shaped welding spots in a longitudinal-type PP. Shirzad et al. [3] found that with increasing inflation height of the channel, Nusselt number increased while pressure drop decreased.

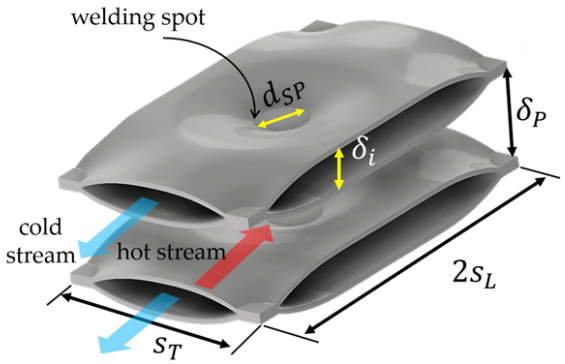

Figure 1: A digital image with the characteristic geometry parameters of PPs. Cold fluid flows through inner channels, hot fluid flows through outer channels [1].

Secondary structuring of surfaces has emerged as a method to further enhance PPHE performance. Djakow

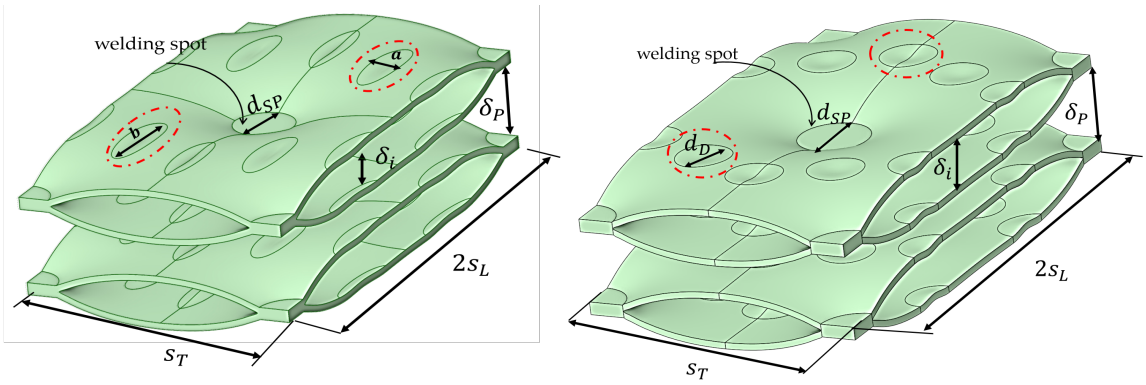

Figure 2: Digital images of the studied PPHEs with secondary structures: streamlined-ellipsoidal (left) and streamlined-spherical (right). Red dashed lines denote the secondary structures.

et al. [4] used electro-incremental hydroforming (EIHF) to apply dimples on PP surfaces; based on numerical simulations, they showed a 24% increase in heat transfer coefficient in an IC of the studied PPHE. Piper et al. [5] demonstrated that dimpled surfaces in the outer channels reduced the negative impact of the recirculation zones and improved efficiency. Afsahnoudeh et al. [1] extended this analysis to a wider range of secondary structures and found that streamlined secondary structures in the outer channels increased thermo-hydraulic efficiency by up to 6%.

Despite these promising results, applying secondary structures on PP surfaces presents challenges, as this method is mainly suitable for simple geometries while surface altering requires a substantial amount of energy (see [6]). Considering these limitations and considering that the main heat transfer resistance can be located in the inner channels [2,3], this work focuses on simple streamlined secondary structures that achieve a balance between performance, manufacturability, and cost. Detailed numerical simulations are conducted to evaluate the effect of secondary structures on flow characteristics and heat transfer efficiency.

GEOMETRY GENERATION AND SURFACE STRUCTURING

To accurately simulate fluid dynamics and heat transfer in the ICs of PPHEs, a realistic digital representation of the PP geometry, which defines the computational domain, is necessary. We employed a forming simulation method detailed in [7] to generate the basic PP geometry. This geometry does not contain secondary structures and serves as a benchmark for the comparison with secondary structured PP. The benchmark has already been optimized with respect to the thermo-hydraulic performance (see [2, 3]).

In our previous work [1], we explored the thermo-hydraulic behavior of the outer channel with different secondary structures. It was found that the PPs with ellipsoidal secondary structures that resulted in a larger volume of the outer channel were most effective in reducing pressure drop and form drag. This geometry, in which both the arrangement and shape of the individual secondary structures are streamlined (Fig. 2, left) is denoted as *streamlined-ellipsoidal*. In [1], we also found that spherical (dimple) secondary structures were most effective in increasing heat transfer, yet with higher pressure drop. Therefore, in this work, we studied two competing PP geometries, the streamlined-ellipsoidal one and the *streamlined-spherical* geometry in which ellipsoidal forms are replaced by spherical forms. The digital images of the two studied secondary structured PPs are shown in Figure 2. In Table 1, the dimensions of the studied PPs are summarized.

Table 1: Geometrical parameters of the studied PPHEs (all dimensions in mm).

d_{SP}	s_L	s_L	δ_i	a	b	d_D
10	36	42	7	4.72	14.2	8.2

CFD MODELING

Model and solution method

The numerical simulations were carried out with the commercial software Fluent 24.1 by ANSYS. The fluid flow was modeled as incompressible, single phase and turbulent, with constant fluid phase properties.

Due to the formation of recirculation zones downstream of the welding spots in an IC and the potential additional recirculation caused by secondary structures, it is crucial to select a turbulence model capable of accurately resolving flow separation. Additionally, the boundary layer separation is expected to induce laminar-turbulent transition. Therefore, to simulate the flow in the IC of the studied PPHEs, we employed the SST model combined with γ (intermittency) transition model [8]. Here, γ

defines the extent of turbulence production in the flow. It has a value of zero for laminar flow, one for fully turbulent flow, and is between zero and one for the transitional flow. The turbulence production term in the SST model equations is multiplied by γ, which allows a smooth transition between laminar and turbulent regimes based on local flow conditions. This model is well suited for resolving separation-induced and crossflow-induced laminar-turbulent transition in complex geometries [8].

The simulation domain and boundary conditions are illustrated in Fig. 3. To reduce the computational effort, we made use of the flow and geometry symmetry by applying symmetric boundary conditions at $y = 0$ and $y = 0.5\ s_T$ (see Fig. 3). No-slip and constant temperature boundary conditions were set at the wall. Additionally, periodic boundary condition was applied at the inlet ($x = 0$) and outlet ($x = 2\ s_L$) boundaries of the channel, while prescribed values of mass flow and constant bulk temperature were given at $x = 0$. Using periodic boundary condition inherently restricts the investigation to the (periodically) fully developed region. Fluent 24.1 utilizes the method introduced by Patankar et al. [9] for simulating problems with periodic boundary conditions.

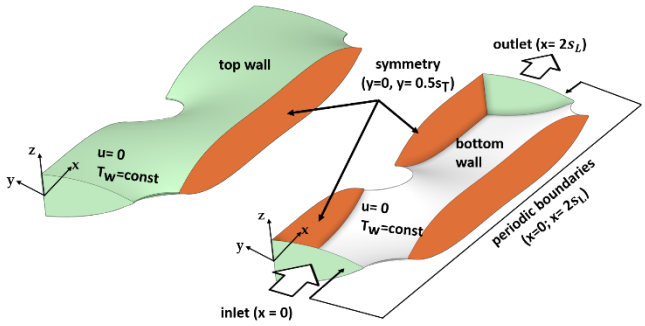

Figure 3: Computational domain and boundary conditions of the PP inner channel.

Grid generation

The grid used was an unstructured poly-hexacore mesh generated with the Fluent-Meshing tool. A grid independence study was performed for all the investigated geometries. Depending on the specific geometry, different grids were generated. The grid was considered finalized when doubling the number of cells resulted in only negligible differences in pressure drop and heat transfer coefficient (less than 0.1%). The number of grid cells ranged between 36 and 42 million. For the finalized grid, the maximum value of the dimensionless wall distance (y^+) was about 0.05.

THERMO-HYDRAULIC EVALUATION CRITERIA

To assess the thermo-hydraulic characteristics of the flow in PPs, the following criteria were used.

The Darcy friction factor ($\xi_{\Delta p}$) can be estimated by the Darcy-Weisbach equation:

$$\xi_{\Delta p} = \frac{2 d_h |\Delta p|}{\rho u_m^2 2 s_L} \quad (1)$$

where u_m is the mean velocity in the IC, d_h is its hydraulic diameter, which can be calculated by the method proposed in [7], and Δp is the overall pressure drop, calculated as the difference between the surface-averaged pressure values at the inlet and outlet boundaries.

Using the Fanning friction factor (ξ_R), determined as

$$\xi_R = \frac{8 \tau_w}{\rho u_m^2} \quad (2)$$

the drag coefficient (ξ_D) is obtained by subtracting Eq. (2) from Eq. (1):

$$\xi_D = \xi_{\Delta p} - \xi_R \quad (3)$$

The Nusselt number is defined by:

$$Nu = \frac{h_m d_h}{\lambda} \quad (4)$$

where λ is thermal conductivity, and h_m represents the surface-averaged heat transfer coefficient which can be calculated as:

$$h_m = \frac{\dot{q}_w}{T_w - T_{bulk}} \quad (5)$$

In Eq. (5), $\dot{q}_w$ is the heat flux in the direction normal to the wall and T_{bulk} is the bulk temperature:

$$T_{bulk} = \frac{\int_{A_{CS}} u T dA}{\int_{A_{CS}} u dA} \quad (6)$$

The thermo-hydraulic efficiency ε is defined as a ratio of the transferred heat per unit time to the pumping power:

$$\varepsilon = \frac{\dot{Q}_w}{\dot{V} \Delta p} \quad (7)$$

where $\dot{V}$ is the volumetric flow rate, and $\dot{Q}_w$ is area-averaged wall heat flux.

The evaluation of the heat transfer coefficient and thermo-hydraulic efficiency of the studied secondary structured PPs is based on the relative deviation of these quantities from the relevant benchmark quantities:

$$Z^* = \frac{Z\ (secondary\ structures) - Z\ (benchmark)}{Z\ (benchmark)} \times 100\% \quad (8)$$

MODEL VALIDATION

The validation of the CFD model was carried out for the benchmark geometry (PPHE without secondary structures). The comparison of the numerical results was performed with the correlations for the Darcy friction factor ($\xi_{\Delta p}$) and the Nusselt number (Nu) from [10].

As can be seen in Fig. 4, $\xi_{\Delta p}$ values obtained from

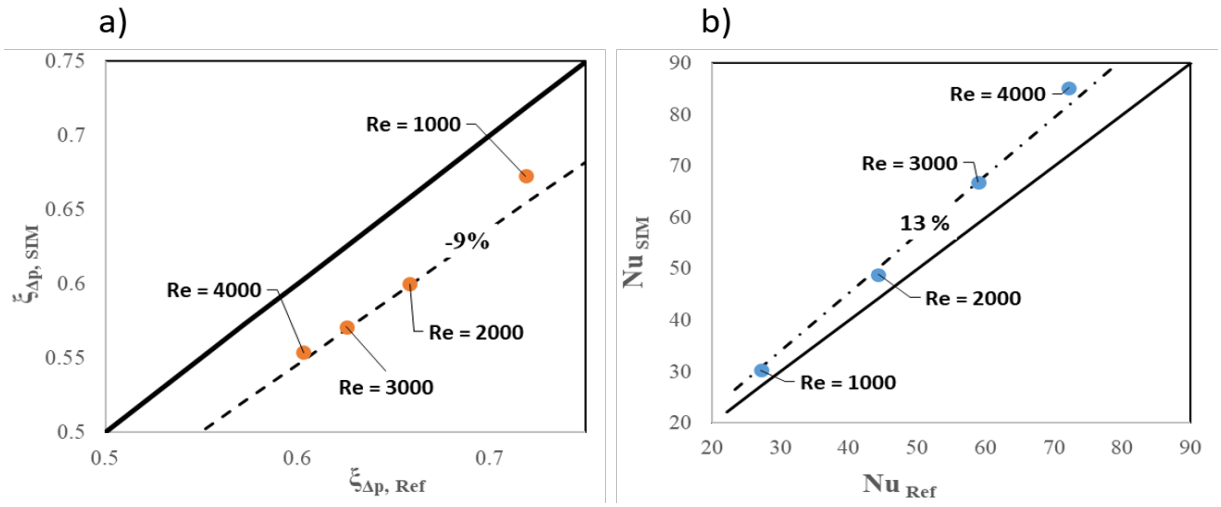

Figure 4: Comparison of simulated Darcy friction factor (a) and Nusselt number (b) with data obtained by correlations from [10].

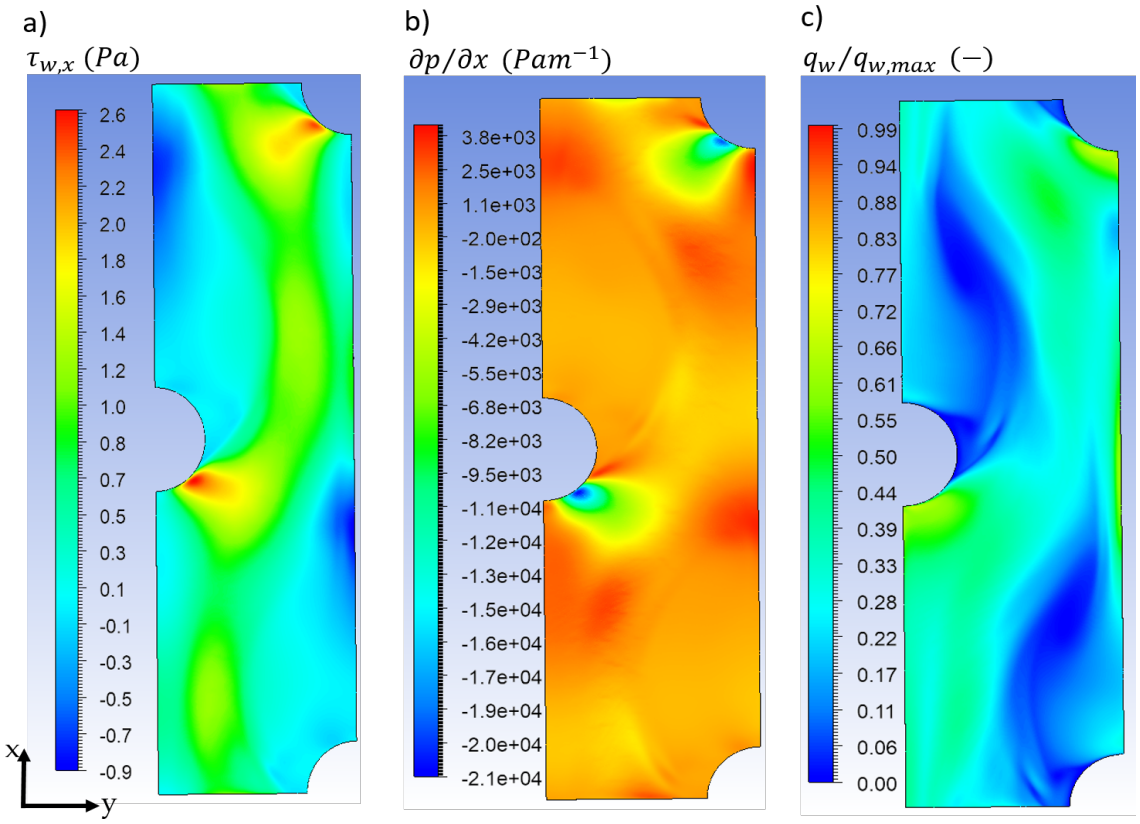

Figure 5: Local wall quantities: shear stress (a), pressure gradient in flow direction (b) and normalized heat flux (c).

the simulation are about 9% lower than the correlation data (Fig. 4a), while Nu values are overestimated by about 13% (Fig. 4b) except for Re = 4000 which shows a higher deviation. Considering that the correlations taken from [10] have an accuracy of ±6% for the Darcy friction factor and ±15% for the Nusselt number, it can be concluded that the simulation results are within the accuracy of the correlations and, hence, the CFD model is validated.

RESULTS AND DISCUSSION

With the validated CFD model, simulations were conducted to investigate the effect of secondary

structures on the flow characteristics and heat transfer. Results were obtained for Reynolds numbers ranging from 1000 to 3000.

In Figure 5, the simulation results of the benchmark IC are shown. The continuous variation in the cross-sectional area of the IC leads to frequent accelerations and decelerations of the flow, resulting in significant changes in wall shear stress (Fig. 5a) along the main flow direction (x-direction). At the maximum inflation height (largest cross-sectional area), the static pressure increases, leading to a positive pressure gradient in the flow direction (Fig. 5b). This causes boundary layer separation and increased form drag. As the flow approaches the welding spot, the cross-sectional area narrows, causing acceleration, a decrease in static pressure, and the development of a negative pressure gradient. The latter reaches its minimum at the stagnation point on the welding spot. Downstream of this point, another boundary layer separation occurs on the welding spot, forming recirculation zones. These zones are the primary contributors to form drag in the IC of the PP. As can be seen in Figure 5c, heat transfer in these recirculation zones is very slow, further emphasizing their detrimental impact on the overall performance.

Figure 6 shows the pressure gradient for the secondary structured PPs. These structures are located in such a way that they are aligned on the maximum inflation height. This alignment mitigates the pressure gradient variations along the main flow, resulting in milder accelerations and decelerations. Consequently, wall friction (Fanning friction factor) and form drag caused by boundary layer separation on the PP surface are reduced. As a result, the overall pressure drop for both secondary-structured PPs is lower than that of the benchmark. This reduction is demonstrated in Figure 7, which shows the Darcy friction factor defined by Eq. (1).

The secondary structures of the streamlined-ellipsoidal PP were most effective in reducing the pressure drop. For a better analysis of the impact of the secondary structures, Figure 8 depicts the Fanning friction factor and drag coefficient. It is evident that the streamlined-ellipsoidal structures primarily influence form drag. The ellipsoidal secondary structures are stretched along the flow direction, which smoothens variations in pressure gradient. This leads to lower wall shear stress (reducing Fanning friction) and minimizes regions with a positive pressure gradient, thereby mitigating boundary layer separation. The latter effect is particularly significant, as the drag coefficient for the streamlined-ellipsoidal PP is approximately 10% lower than that of the benchmark. The results for the streamlined-spherical PP reveal a different behavior compared to the streamlined-ellipsoidal design. While the Fanning friction factor remains nearly the same as for the benchmark, the drag coefficient is reduced by approximately 4%. For both secondary structured PPs, the drag coefficient was lowest at $Re = 2000$.

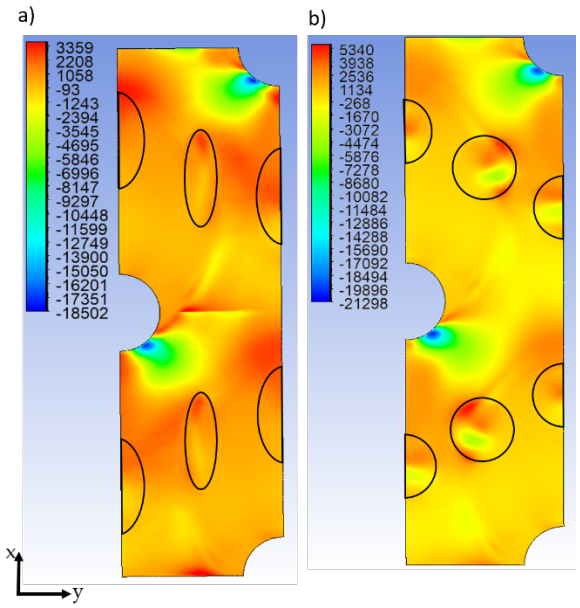

Figure 6: Pressure gradient in flow direction for different PPs: streamlined-ellipsoidal (a); streamlined-spherical (b). The secondary structures are denoted with black contours.

In Figure 9, the heat transfer coefficients of the secondary-structured PPs relative to the benchmark (h^*) are shown. While the streamlined-ellipsoidal PP effectively reduced the pressure drop, its heat transfer coefficient was lower due to lower wall friction and fluid mixing in the boundary layer. In contrast, the streamlined-spherical PP achieved higher heat transfer rate by enhancing fluid mixing in the boundary layer.

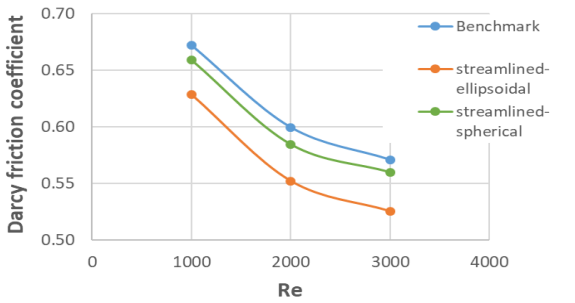

Figure 7: Darcy friction factor for studied PPHEs

From an industrial perspective, the thermo-hydraulic efficiency ε defined by Eq. (7) provides a more meaningful performance evaluation. As shown in Figure 10, the streamlined-ellipsoidal PP consistently achieves a significant enhancement of thermo-hydraulic efficiency relative to benchmark (ε^*) across the entire range of studied Reynolds numbers. This indicates that the "more streamlined" secondary structures are more effective and show a high potential for optimizing the thermo-hydraulic

efficiency of PPHEs.

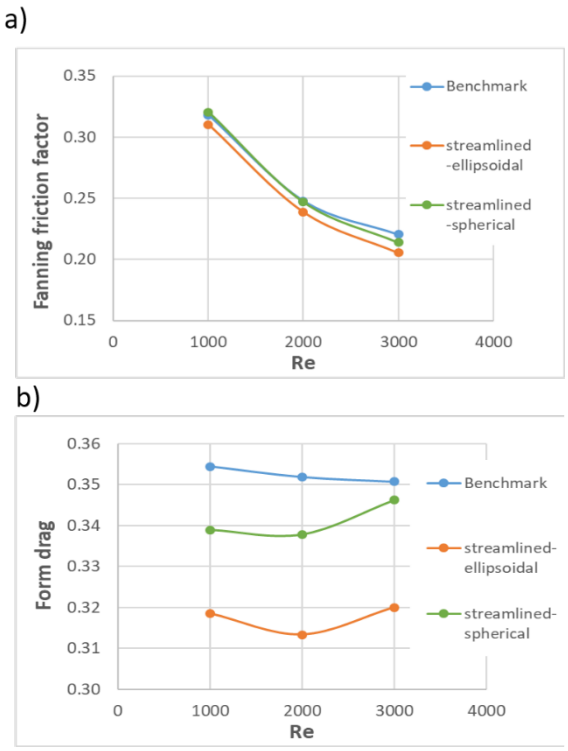

Figure 8: Friction coefficients: Fanning friction factor (a) and drag coefficient (b) for studied PPHEs.

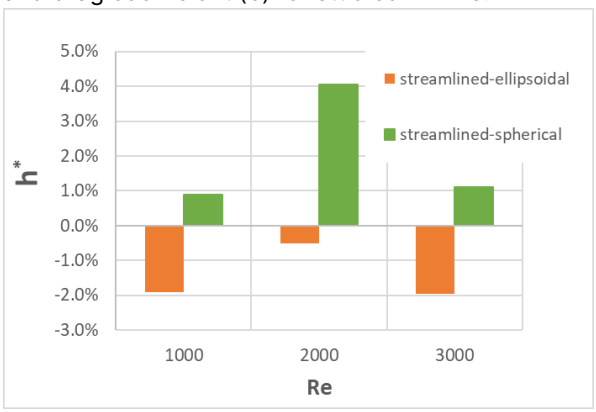

Figure 9: Heat transfer coefficient of the studied structured PPs relative to benchmark.

CONCLUSION

In this work, a CFD-based study was conducted to analyse fluid flow and heat transfer in the inner channel (IC) of pillow-plate heat exchangers (PPHEs) with streamlined secondary structuring. Two designs, streamlined-ellipsoidal and streamlined-spherical, were compared with a benchmark representing an optimized PPHE geometry without secondary structures.

The streamlined-ellipsoidal design resulted in a significantly reduced pressure drop by minimizing boundary layer separation and levelling out pressure variations along the main flow direction. However, its streamlined shape resulted in lower near-wall mixing, and hence, lower heat transfer coefficient compared to the benchmark. In contrast, the streamlined-spherical design enhanced heat transfer by improving near-wall mixing but offered a lower reduction in pressure drop.

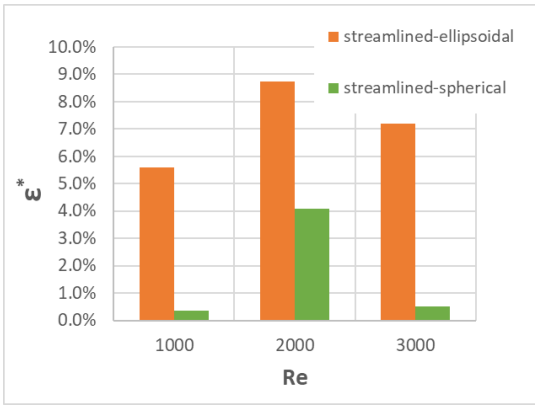

Figure 10: Thermo-hydraulic efficiency of the studied structured PPs relative to benchmark.

The overall performance was evaluated using thermo-hydraulic efficiency. The streamlined-ellipsoidal design outperformed both the benchmark and the streamlined-spherical design for all studied Reynolds numbers. This clearly highlights the potential of the streamlined secondary structures in optimizing the performance of the PPHEs.

Future work will focus on investigating the combined impact of secondary structuring on both inner and outer PPHE channels to allow a comprehensive optimization.

ACKNOWLEDGEMENTS

The authors are grateful for the financial support from the German Research Foundation (DFG, Project number KE 837/46-1). Furthermore, the authors gratefully acknowledge the funding of this project by computing time provided by the Paderborn Center for Parallel Computing (PC^2).

REFERENCES

1. Afsahnoudeh R., Wortmeier A., Holzmüller M., Gong Y., Homberg W., Kenig E.Y. Thermo-hydraulic performance of pillow-plate heat exchangers with secondary structuring: A numerical analysis, *Energies* 16(21):7284 (2023)
2. Piper M., Zibart A., Tran J.M., Kenig E.Y. Numerical investigation of turbulent forced convection heat transfer in pillow plates, *Int. J. Heat Mass Transfer*, 94:516–527 (2016)
3. Shirzad M., Mousavi Ajarostaghi S. S., Aghajani

Delavar M., Sedighi K. Improve the thermal performance of the pillow plate heat exchanger by using nanofluid: Numerical simulation, *Adv. Powder Technol.* 30:1356-1365 (2019)
4. Djakow E., Springer R., Homberg W., Piper M., J Tran J.M, Zibart A., Kenig E.Y. Incremental electrohydraulic forming - A new approach for the manufacturing of structured multifunctional sheet metal blanks, Proc. of the 20th International ESAFORM Conference on Material Forming (2017)
5. Piper M., Zibart A., Djakow E., Springer R., Homberg W., Kenig E. Y. Heat transfer enhancement in pillow-plate heat exchangers with dimpled surfaces: A numerical study. *Appl. Therm. Eng*. 153:142–146 (2019)
6. Hosford W.F., Caddell R.M. Metal Forming Mechanics and Metallurgy, Cambridge University Press (2011)
7. Piper M., Olenberg A., Tran J.M., Kenig E.Y. Determination of the geometric design parameters of pillow-plate heat exchangers *Appl. Therm. Eng.* 91:1168–1175 (2015)
8. Menter F.R., Smirnov P.E., Liu T., Avancha R. A one-equation local correlation-based transition model, *Flow Turbulence Combust* 95:583–619 (2015).
9. Patankar S. V., Liu C. H., Sparrow E. M. Fully developed flow and heat transfer in ducts having streamwise-periodic variations of cross-sectional area, *ASME J. Heat Transfer* 99:180-186 (1977)
10. Piper M., Zibart A., Tran J.M., Kenig E.Y. New design equations for turbulent forced convection heat transfer and pressure loss in pillow-plate channels *Int. J. Therm. Sci.* 120:459-468 (2017)